



Turing pattern dynamics in a fractional-diffusion oregonator model under PD control*

Hongliang Li^a, Yi Yao^b, Min Xiao^{a, 1}, Zhen Wang^c,
Leszek Rutkowski^d

^a College of Automation & College of Artificial Intelligence,
Nanjing University of Posts and Telecommunications,
Nanjing 210023, China
1541465904@qq.com; candymanxm2003@aliyun.com

^b School of Mathematical Sciences,
Nanjing Normal University,
Nanjing 210023, China
05302@njnu.edu.cn

^c College of Mathematics and Systems Science,
Shandong University of Science and Technology,
Qingdao 266590, China
wangzhen@sdust.edu.cn

^d Systems Research Institute of the Polish Academy of Sciences,
01-447 Warsaw, Poland
leszek.rutkowski@ibspan.waw.pl

Received: June 20, 2024 / **Revised:** January 8, 2025 / **Published online:** February 26, 2025

Abstract. In this paper, fractional-order diffusion and proportional-derivative (PD) control are introduced in oregonator model, and the Turing pattern dynamics is investigated for the first time. We take the cross-diffusion coefficient as the bifurcation parameter and give some necessary conditions for Turing instability of the fractional-diffusion oregonator model under PD control. At the same time, we construct the amplitude equations near the bifurcation threshold and determine the pattern formation of the fractional-diffusion oregonator model under PD controller. It is observed by numerical simulations that in the absence of control, the pattern formation changes with the variation of the cross-diffusion coefficient in two-dimensional space. Meanwhile, it is verified that the PD control has a significant impact on Turing instability, and the pattern structure can be changed by manipulating the control gain parameters for the fractional-diffusion oregonator model.

Keywords: PD controller, cross diffusion, fractional diffusion, Turing pattern, oregonator model.

*This research was supported by the National Natural Science Foundation of China (62073172) and the Natural Science Foundation of Jiangsu Province of China under grant BK20221329.

¹Corresponding author.

1 Introduction

In the 1940s, Turing discovered that a nonlinear reaction–diffusion model could give rise to stable spatial patterns from his research [22]. This phenomenon is called diffusion-driven instability. Apparently, a typical Turing system consists of at least two chemical reactants, usually called activator and inhibitor. In the absence of diffusion, their steady state is stable with small perturbations. But in the case of diffusion, they become unstable. Usually, when a substance diffuses, its concentration gradient decreases, thereby eliminating any structure. However, in Turing instability, diffusion is precisely the reason why the system loses its stable uniform state and exhibits a structural pattern [2, 7, 8, 14, 30].

Based on Turing's theoretical research, many scholars have proposed a series of reaction–diffusion models, such as Belousov–Zhabotinsky reaction model, Degn–Harrison model, Gray–Scott model, Gierer–Meinhardt model, etc. [10, 11, 17, 29, 31]. They have studied the Turing instability and pattern formation of these models in depth. Some results obtained from these reaction–diffusion models have important guiding significance for explaining some strange phenomenon in nature.

Specifically, in 1974, Field et al. [10] proposed a simplified version of three-variable Belousov–Zhabotinsky chemical reaction model on the basis of the existing theoretical research and called it oregonator model. According to the actual chemical reaction, Yyson et al. [23] further simplified it into a more operable bivariate oregonator model. Since then, the research on this chemical reaction model has been more and more in depth. Bhuvanewari et al. [5] studied the Turing instability of oregonator model after introducing the self-diffusion term through linear stability analysis. Peng et al. [19] further obtained the conditions under which the self-diffusion term drives the generation of Turing patterns in oregonator model, and gave some threshold conditions that may generate different Turing patterns.

In fact, it is found that the effect of cross-diffusion terms on bifurcation kinetics and mode formation of reaction–diffusion models plays a significant role in chemical reaction models [20, 21, 24]. Igal et al. [4] studied the Turing instability of oregonator model driven by cross diffusion and the influence of cross-diffusion term on the Turing mode of the model under different system parameters. In particular, they provided some parameter conditions required for the formation of special Turing pattern. Berenstein et al. [3] revealed some special behavior patterns induced by cross-diffusion terms in the oregonator model. Including Turing patterns, standing waves, oscillatory Turing patterns, and quasistanding waves and other patterns need to meet the threshold conditions.

Moreover, Voroney et al. [27] found that the nature of the medium in which reaction and diffusion processes occur can influence the character of spatiotemporal dynamics that is observed. Furthermore, diffusion process can be affected by the make-up of the medium and its geometry [12, 25, 26]. In this case, it leads to the change of Turing pattern in the reaction–diffusion model comparing with general situation. In general, the reaction–diffusion equation describes the molecule performing a nearest neighbor jump at a site. The mean-square displacement of the molecule changes over time: $\Delta r^2 \sim t^\gamma$. When $\gamma = 1$, system experiences normal diffusion; when $\gamma \neq 1$, system experiences abnormal

diffusion [9, 13]. The abnormal diffusion corresponds to the fractional-diffusion index. This situation generally appears in some fractal media, which means the jump amplitude and jump waiting time of the molecule change. Some scholars had studied the influence of diffusion index on the formation of system patterns in reaction–diffusion models and made some achievements. Golovin et al. [18] found through experiments that when the diffusion index of reaction–diffusion models is fractional, the formation of patterns does not necessarily depend on the specific size relationship between the diffusion rates of activator and inhibitor. Langlands et al. [16] investigated a system with abnormal diffusion and concluded that when the diffusion index of activator is equal to the diffusion index of inhibitor, the formation conditions of Turing patterns are the same as those of normal reaction–diffusion model. In general, considering anomalous diffusion plays an important role in exploring the dynamics of pattern formation in fractal media. Feng et al. [9] researched the effect of the partial derivative order of the self-diffusion term on the Turing mode of the model and gave the change relationship between the Turing stability of the model and the superdiffusion term.

Also, in recent years, the research on control strategies has developed rapidly and been widely applied in many fields, including biology, medicine, computer science, etc. [1, 15, 34]. Especially, Xu et al. [28] built a novel plankton population delayed dynamical model and designed a suitable nonlinear delay feedback controller and a reasonable hybrid controller, obtaining the critical delay value to control the stability domain and the time of appearance of bifurcation phenomenon of the formulated plankton population delayed dynamical model. Moreover, Zhao et al. [32] proposed a novel delayed Lotka–Volterra commensal symbiosis model and developed two distinct hybrid delayed feedback controllers, successfully modifying the domain of stability and the time of the bifurcation phenomenon in this model. The results referring above may be used for other fractional-order and integer-order dynamical systems in a wide range of disciplines to dominate the bifurcation phenomena, stability, and chaos. In fact, the proportional-derivative (PD) controller is a hybrid control strategy that has been proved to be effective at present. It has the advantages of improving the response speed of the system and reducing the oscillation. Ding et al. [6] applied PD control strategy to the small-world network model to effectively suppress Hopf bifurcation of the model. Zhu et al. [33] used PD control strategy in the diffused mussel–algae model to effectively suppress the Turing instability of the model and ensure the stability of the model.

Based on some inspirations from the above research, this paper introduces PD controller to realize effective regulation of fractional-order diffusion oregonator model. We first discuss the effect of fractional-diffusion index on system pattern formation, then we study the effect of PD controller on the Turing instability of oregonator model and use PD controller to drive the pattern structures of the model to change so that the Turing unstable state can be restored to a stable state.

The specific organization of this paper is as follows. In Section 2, we present the studied bivariate oregonator model with cross-diffusion terms and introduce the PD controller used and fractional-order diffusion. In Section 3, we analyze the threshold conditions for Turing instability in the model. In Section 4, the amplitude equation of the model is given and analyzed theoretically. In Section 5, we give the stability conditions of different

patterns. In Section 6, we perform some numerical simulations in two-dimensional space. In Section 7, the conclusions are drawn.

2 Model description

Oregonator reaction model is a kinetic model used to describe the interaction of several types of chemical substances, as follows [5]:

$$\frac{du}{dt} = \frac{1}{a} \left[u - u^2 - fv \frac{u - q}{u + q} \right], \quad \frac{dv}{dt} = u - v, \quad (1)$$

where u represents the dimensionless concentration of HBrO_2 , and v represents the concentration of Ce^{a+} . a is the ratio of the time scale. f is the ratio of bromine and dibromomalonic acid in the reaction model, and its value is related to the initial conditions. q is related to some kinetic parameters and the initial concentration of the reagent.

According to mathematical analysis, there is a unique positive equilibrium

$$E^* = (u^*, v^*) = \left(\frac{-b + \sqrt{b^2 + 4c}}{2}, \frac{-b + \sqrt{b^2 + 4c}}{2} \right),$$

where $b = f + q - 1$, $c = fq + q$.

We introduce the following PD controller into the model

$$F = k_p(v - v^*) + k_d \frac{d(v - v^*)}{dt}$$

in which k_p and k_d indicate the proportional coefficient and the differential coefficient, respectively.

So the controlled oregonator model can be expressed as follows:

$$\frac{du}{dt} = \frac{1}{a} \left[u - u^2 - fv \frac{u - q}{u + q} \right], \quad \frac{dv}{dt} = u - v + F. \quad (2)$$

Obviously, the equivalent form of model (2) is as follows:

$$\frac{du}{dt} = \frac{1}{a} \left[u - u^2 - fv \frac{u - q}{u + q} \right], \quad \frac{dv}{dt} = \frac{u - v + k_p(v - v^*)}{1 - k_d}. \quad (3)$$

Then we introduce the fractional-order diffusion terms into the controlled model (3) and obtain

$$\begin{aligned} \frac{\partial u}{\partial t} &= \frac{1}{a} \left[u - u^2 - fv \frac{u - q}{u + q} \right] + D_u \nabla^\alpha u + D_{uv} \nabla^\alpha v, \\ \frac{\partial v}{\partial t} &= \frac{u - v + k_p(v - v^*)}{1 - k_d} + D_{vu} \nabla^\alpha u + D_v \nabla^\alpha v, \\ \frac{\partial u}{\partial \eta} &= \frac{\partial v}{\partial \eta} = 0, \\ u(x, y, 0) &> 0, \quad v(x, y, 0) > 0, \end{aligned} \quad (4)$$

D_u, D_v are the self-diffusion coefficients, and D_{uv}, D_{vu} are the cross-diffusion coefficients. η is the outward unit normal vector of the boundary. The homogeneous Neumann boundary condition indicates that this model is self-contained with zero flux across the boundary. ∇^α is the fractional-order Laplace operator, and $1 < \alpha \leq 2$. The form of fractional-order diffusion term for u (the same form for v) can be defined as

$$\nabla^\alpha u = -\frac{\sec \bar{\alpha}}{2\Gamma(2 - \alpha)} \frac{d^2}{dx^2} \int_{-\infty}^{+\infty} \frac{u(\xi, t)}{(x - \xi)^{\alpha-1}} d\xi,$$

where $\bar{\alpha} = \pi\alpha/2$, and $\Gamma(\cdot)$ denotes the Gamma function.

Considering that all eigenvalues of the diffusion matrix of a chemical model must be positive, the following assumption is made:

$$(H_1) \quad \begin{aligned} D_u, D_v > 0, \quad (D_u + D_v)^2 - 4(D_u D_v - D_{uv} D_{vu}) \geq 0, \\ D_u D_v - D_{uv} D_{vu} > 0. \end{aligned}$$

Analyzing the effect of the diffusion terms on the Turing instability of the model, assumption (H₁) needs to always be true.

3 Analysis of local stability and Turing instability

In this section, we firstly investigate the local stability of the nondiffusive model (3) at the equilibrium point. Then, on the basis of local asymptotic stability of the nondiffusive model (3), we study the Turing instability at the equilibrium point of the fractional-diffusion model (4), and the Turing bifurcation threshold condition is given by selecting bifurcation parameter.

3.1 Local stability for the nondiffusive model (3)

It is clearly that the nondiffusive model (3) and model (1) have the commonly unique positive equilibrium E^* . For the nondiffusive model (3), linearization is performed at the equilibrium point E^* , resulting in the corresponding Jacobian matrix J as follows:

$$J = \begin{bmatrix} e_{11} & e_{12} \\ \frac{e_{21}}{1-k_d} & \frac{e_{22}+k_p}{1-k_d} \end{bmatrix}$$

in which

$$\begin{aligned} e_{11} &= \frac{1 - 2u^*}{a} - \frac{2fqv^*}{a(u^* + q)^2}, & e_{12} &= \frac{f(u^* - q)}{a(u^* + q)}, \\ e_{21} &= 1, & e_{22} &= -1. \end{aligned}$$

The characteristic equation of model (3) is

$$\lambda^2 + p_0\lambda + h_0 = 0, \tag{5}$$

where

$$p_0 = -\left(e_{11} + \frac{e_{22} + k_p}{1 - k_d} \right), \quad h_0 = \frac{e_{11}(e_{22} + k_p)}{1 - k_d} - \frac{e_{12}e_{21}}{1 - k_d},$$

and the eigenvalues calculated from Eq. 5 are provided by

$$\lambda_{1,2} = \frac{-p_0 \pm \sqrt{p_0^2 - 4h_0}}{2}.$$

We propose the following assumption:

$$(H_2) \quad \frac{2u^* - 1}{a} + \frac{2fqv^*}{a(u^* + q)^2} - \frac{k_p - 1}{1 - k_d} > 0,$$

$$\left[\frac{1 - 2u^*}{a} - \frac{2fqv^*}{a(u^* + q)^2} \right] \frac{k_p - 1}{1 - k_d} - \frac{f(u^* - q)}{a(u^* + q)(1 - k_d)} > 0.$$

Theorem 1. *If (H₂) always holds, then model (3) is locally asymptotically stable at the equilibrium point E*.*

Proof. If (H₂) holds, we have p₀ > 0, h₀ > 0. Then we easily obtain λ_{1,2} < 0. According to sufficient conditions for the stability of linear systems and the topological classification of hyperbolic equilibrium points plane, it is easily concluded that E* is locally asymptotically stable. □

Remark 1. It should be noted that Turing instability corresponds to diffusion-driven instability in a uniform steady state. That is, in a uniformly stirred model without the drive of diffusion terms, it remains stable. But in a complete reaction–diffusion model, it is unstable. So it is necessary to ensure that model (3) remains stable at the equilibrium point E*.

3.2 Turing instability for the fractional-diffusion model (4)

Assuming that the perturbation form at the equilibrium point E* can be written as e^{λt} × cos k_xx cos k_yy, by conducting a perturbation analysis at equilibrium point E*, the Jacobian matrix J_k for the fractional-diffusion model (4) is as follows:

$$J_k = \begin{bmatrix} e_{11} - k^\alpha D_u & e_{12} - k^\alpha D_{uv} \\ \frac{e_{21}}{1 - k_d} - k^\alpha D_{vu} & \frac{e_{22} + k_p}{1 - k_d} - k^\alpha D_v \end{bmatrix},$$

where k is the wave number. From the Jacobian matrix the characteristic equation of model (4) is obtained as follows:

$$\lambda^2 + p_k \lambda + h_k = 0, \tag{6}$$

where

$$\begin{aligned}
 p_k &= k^\alpha(D_u + D_v) + p_0, \\
 h_k &= (D_u D_v - D_{uv} D_{vu})k^{2\alpha} \\
 &+ \left(-D_u \frac{e_{22} + k_p}{1 - k_d} - D_v e_{11} + D_{uv} \frac{e_{21}}{1 - k_d} + D_{vu} e_{12} \right) k^\alpha + h_0,
 \end{aligned}$$

and the eigenvalues calculated from Eq. 6 are provided by

$$\lambda_{3,4} = \frac{-p_k \pm \sqrt{p_k^2 - 4h_k}}{2}.$$

For the sake of convenience, we let

$$\begin{aligned}
 d &= D_u D_v - D_{uv} D_{vu}, \\
 g &= -D_u \frac{e_{22} + k_p}{1 - k_d} - D_v e_{11} + D_{uv} \frac{e_{21}}{1 - k_d} + D_{vu} e_{12}.
 \end{aligned}$$

In order to explain the conditions of Turing instability in the model, we propose the following assumption:

$$(H_3) \quad g < 0, \quad \Delta = g^2 - 4dh_0 > 0.$$

Theorem 2. *If (H₁)–(H₃) hold, then model (4) undergoes Turing instability at the equilibrium point E*.*

Proof. Equation (6) has provided the characteristic relation of model (4) including diffusion terms. If (H₁)–(H₃) hold, we have $p_k > 0$ and $h_k < 0$, obtaining $\lambda_3 = (-p_k - \sqrt{p_k^2 - 4h_k})/2 < 0$ and $\lambda_4 = (-p_k + \sqrt{p_k^2 - 4h_k})/2 > 0$. According to Theorem 1, it is verified that E^* is unstable, so that model (4) undergoes Turing instability. \square

Obviously, h_k is a quadratic function of k^α . If (H₃) holds, we can drive the conclusion that $h_k < 0$ holds for some certain values of k .

For $h_k = 0$, we obtain k_t for the lowest point of it as follows:

$$k_t = \left(\frac{-D_u \frac{e_{22} + k_p}{1 - k_d} - D_v e_{11} + D_{uv} \frac{e_{21}}{1 - k_d} + D_{vu} e_{12}}{2(D_{uv} D_{vu} - D_u D_v)} \right)^{1/\alpha}.$$

Then we get that

$$h_{k_{\min}} = h_0 - \frac{\left(-D_u \frac{e_{22} + k_p}{1 - k_d} - D_v e_{11} + D_{uv} \frac{e_{21}}{1 - k_d} + D_{vu} e_{12} \right)^2}{4(D_u D_v - D_{uv} D_{vu})}.$$

By Theorem 2, the Turing instability condition of model (4) turns into the following inequality:

$$h_{k_{\min}} < 0.$$

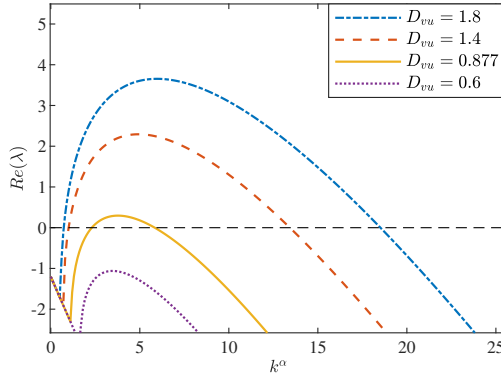


Figure 1. The graphic of $Re(\lambda)$ against k^α for $D_{vu} = 0.6, 0.877, 1.4,$ and 1.8 .

Choosing D_{vu} as the bifurcation parameter of model (4), we give the critical value for Turing instability of D_{vu} as follows:

$$\begin{aligned}
 D_{vu}^T = & \frac{1}{e_{12}^2} [D_v e_{11} e_{12} - 2D_{uv} e_{11} e_{22} + D_u e_{12} e_{22} - 2D_{uv} e_{11} k_p \\
 & + D_u e_{12} k_p - 2((D_{uv} e_{11} - D_u e_{12})(D_{uv} e_{22} - D_v e_{12} + D_{uv} k_p) \\
 & \times (e_{11} e_{22} - e_{12} e_{21} + e_{11} k_p))^{1/2}]. \tag{7}
 \end{aligned}$$

Then we supply some numerical simulations to verify our theoretical analysis of Turing instability for model (4). The parameters are selected as: $a = 0.04, q = 0.01, f = 0.5,$ and $k_d = k_p = 0$. Through calculation, we determine that the equilibrium point $E^* = (u^*, v^*) = (0.5189, 0.5189)$. We let $D_u = D_v = 1, D_{uv} = 0$ and select D_{vu} as the bifurcation parameter, obtaining the Turing bifurcation parameter $D_{vu}^T = 0.8098$ from Eq. (7).

We fit the graph of the relationship between $Re(\lambda)$ and k^α as shown in Fig. 1. It is obviously that when $D_{vu} > D_{vu}^T$, Eq. (6) has the characteristic roots with positive real parts. In Fig. 1, as the value of D_{vu} increases, the range of k^α that makes $Re(\lambda)$ positive gradually expands. It means that Turing instability becomes more likely to occur. Also, we can see that when $D_{vu} < D_{vu}^T$, $Re(\lambda)$ always keeps negative. In this case, Turing instability does not occur in model (4).

We also simulate how different values of α influence the relationship between $Re(\lambda)$ and k in Fig. 2. Also, the relationship between k_t and α for $D_{vu} = 1.8$ is plotted in Fig. 3. We can see from Fig. 2 that when D_{vu} is fixed, changing the value of α does not influence the maximum of $Re(\lambda)$. But as α decreases, the wave number's range of Turing instability expands. Specifically, when α is smaller, $Re(\lambda) > 0$ will appear earlier and disappear later. Meanwhile, the value of critical wave number k_t decreases when α decreases as shown in Fig. 3. Figures 2 and 3 indicate that when choosing smaller value of α , model (4) is more likely to generate Turing instability.

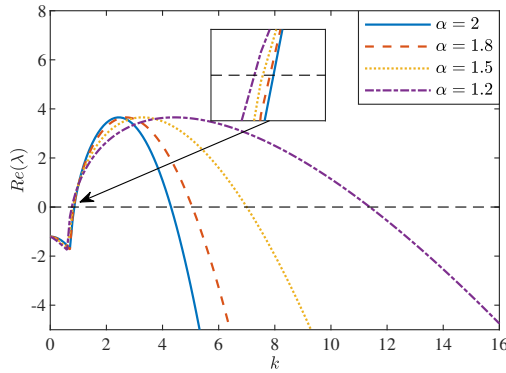


Figure 2. The graphic of $Re(\lambda)$ against k for $D_{vu} = 1.8$ and the parameters $\alpha = 2, 1.8, 1.5, 1.2$.

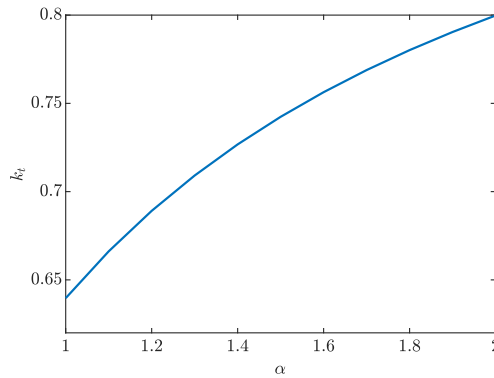


Figure 3. The graphic of k_t against α for $D_{vu} = 1.8$.

4 Weakly nonlinear analysis

In this section, we apply amplitude equations to explore the different pattern formations in model (4). By applying the standard multiscale analysis, we derive the amplitude equations for the occurrence of Turing instability.

First, expanding model (4) by Taylor expansion around the homogeneous steady state $E^* = (u^*, v^*)$, we get

$$\frac{\partial}{\partial t} \begin{pmatrix} \hat{u} \\ \hat{v} \end{pmatrix} = L \begin{pmatrix} \hat{u} \\ \hat{v} \end{pmatrix} + N, \tag{8}$$

where

$$L = \begin{pmatrix} D_u \nabla^\alpha + e_{11} & D_{uv} \nabla^\alpha + e_{12} \\ D_{vu} \nabla^\alpha + \frac{e_{21}}{1-k_d} & D_v \nabla^\alpha + \frac{e_{22}+k_p}{1-k_d} \end{pmatrix},$$

$$N = \begin{pmatrix} p_{20} \hat{u}^2 + p_{11} \hat{u} \hat{v} + p_{02} \hat{v}^2 \\ q_{20} \hat{u}^2 + q_{11} \hat{u} \hat{v} + q_{02} \hat{v}^2 \end{pmatrix} + \begin{pmatrix} p_{30} \hat{u}^3 + p_{21} \hat{u}^2 \hat{v} + p_{12} \hat{u} \hat{v}^2 + p_{03} \hat{v}^3 \\ q_{30} \hat{u}^3 + q_{21} \hat{u}^2 \hat{v} + q_{12} \hat{u} \hat{v}^2 + q_{03} \hat{v}^3 \end{pmatrix}$$

in which

$$\begin{aligned}
 p_{11} &= \frac{25(u^* - \frac{1}{100})}{2(u^* + \frac{1}{100})^2} - \frac{25}{2(u^* + \frac{1}{100})}, \\
 p_{20} &= \frac{25v^*}{2(u^* + \frac{1}{100})^2} - \frac{25v^*(u^* - \frac{1}{100})}{2(u^* + \frac{1}{100})^3} - 25, \\
 p_{21} &= \frac{25}{2(u^* + \frac{1}{100})^2} - \frac{25(u^* - \frac{1}{100})}{2(u^* + \frac{1}{100})^3}, \\
 p_{30} &= \frac{25v^*(u^* - \frac{1}{100})}{2(u^* + \frac{1}{100})^4} - \frac{25v^*}{2(u^* + \frac{1}{100})^3}, \\
 p_{02} &= p_{03} = p_{12} = 0, \\
 q_{02} &= q_{03} = q_{11} = q_{12} = q_{20} = q_{21} = q_{30} = 0.
 \end{aligned}$$

For simplicity of writing, we still replace $(\hat{u} \ \hat{v})^\top$ with $(u \ v)^\top$ in the following.

Because in the calculation, the analysis is limited to the behavior of the control parameters near the critical point of the phase transition, we expand D_{vu} in the following way:

$$D_{vu}^T - D_{vu} = \varepsilon d_1 + \varepsilon^2 d_2 + \varepsilon^3 d_3 + o(\varepsilon^3), \tag{9}$$

where ε is taken as a small quantity. Use this small parameter ε to expand the variable $(u \ v)^\top$ and the nonlinearity N as follows:

$$\begin{pmatrix} u \\ v \end{pmatrix} = \varepsilon \begin{pmatrix} u_1 \\ v_1 \end{pmatrix} + \varepsilon^2 \begin{pmatrix} u_2 \\ v_2 \end{pmatrix} + \varepsilon^3 \begin{pmatrix} u_3 \\ v_3 \end{pmatrix} + o(\varepsilon^3), \tag{10}$$

and

$$N = \varepsilon^2 N_2 + \varepsilon^3 N_3 + o(\varepsilon^3), \tag{11}$$

where

$$\begin{aligned}
 N_2 &= \begin{pmatrix} p_{20}u_1^2 + p_{11}u_1v_1 \\ 0 \end{pmatrix}, \\
 N_3 &= \begin{pmatrix} 2p_{20}u_1u_2 + p_{11}u_1v_2 + p_{11}u_2v_1 + 2p_{02}v_1v_2 \\ 0 \end{pmatrix} + \begin{pmatrix} p_{30}u_1^3 + p_{21}u_1^2v_1 \\ 0 \end{pmatrix}.
 \end{aligned}$$

The linear operator L can be decomposed into

$$L = L_c + (D_{vu} - D_{vu}^T)M, \tag{12}$$

where

$$L_c = \begin{pmatrix} D_u \nabla^\alpha + e_{11} & D_{uv} \nabla^\alpha + e_{12} \\ D_{vu}^T \nabla^\alpha + \frac{e_{21}}{1-k_d} & D_v \nabla^\alpha + \frac{e_{22}+k_p}{1-k_d} \end{pmatrix}, \quad M = \begin{pmatrix} 0 & 0 \\ \nabla^\alpha & 0 \end{pmatrix}.$$

Separating the dynamical scales of the model, we let $t_1 = \varepsilon t$, $t_2 = \varepsilon^2 t$, $t_3 = \varepsilon^3 t$ and treat them as independent variables. Then the micro quotient as regards t can be written as

$$\frac{\partial}{\partial t} = \varepsilon \frac{\partial}{\partial t_1} + \varepsilon^2 \frac{\partial}{\partial t_2} + \varepsilon^3 \frac{\partial}{\partial t_3} + o(\varepsilon^3). \tag{13}$$

By substituting Eqs. (9)–(13) into Eq. (8), according to the different orders of ε , we obtain the corresponding perturbation equations

$$\varepsilon: L_c \begin{pmatrix} u_1 \\ v_1 \end{pmatrix} = \mathbf{0}, \tag{14}$$

$$\varepsilon^2: L_c \begin{pmatrix} u_2 \\ v_2 \end{pmatrix} = \frac{\partial}{\partial t_1} \begin{pmatrix} u_1 \\ v_1 \end{pmatrix} - d_1 M \begin{pmatrix} u_1 \\ v_1 \end{pmatrix} - N_2, \tag{15}$$

$$\varepsilon^3: L_e \begin{pmatrix} u_3 \\ v_3 \end{pmatrix} = \frac{\partial}{\partial t_1} \begin{pmatrix} u_2 \\ v_2 \end{pmatrix} + \frac{\partial}{\partial t_2} \begin{pmatrix} u_1 \\ v_1 \end{pmatrix} - d_2 M \begin{pmatrix} u_1 \\ v_1 \end{pmatrix} - d_1 M \begin{pmatrix} u_2 \\ v_2 \end{pmatrix} - N_3. \tag{16}$$

For perturbation equations, we usually describe their solutions in terms of modulus. The modulus includes three wave vectors called k_1 , k_2 , and k_3 , respectively. The intersection angle of the wave vectors is 120° .

Solving Eq. (14), we have

$$\begin{pmatrix} u_1 \\ v_1 \end{pmatrix} = \begin{pmatrix} \varphi \\ 1 \end{pmatrix} \left(\sum_{j=1}^3 W_j e^{i k_j \cdot r} + \text{c.c.} \right), \quad j = 1, 2, 3, \tag{17}$$

where c.c. denotes the complex conjugate, and $r = (x, y)$ stands for the spatial vector. W_j is the amplitude of $e^{i k_j \cdot r}$. Meanwhile,

$$\varphi = \frac{D_{vu}^T k_c^\alpha - e_{12}}{e_{11} - D_u k_c^\alpha}, \quad |k_j| = k_c, \quad k_c^\alpha = k_t^\alpha (D_{vu}^T).$$

On account of Fredholm solvability condition, the right-hand side of Eqs. (14)–(16) must be orthogonal to the eigenvectors of the zero eigenvalue of L_c^* , which is the adjoint operator of L_c . The eigenvectors of L_c^* can be written as

$$\begin{pmatrix} 1 \\ \psi \end{pmatrix} e^{i k_j \cdot r} + \text{c.c.}, \quad j = 1, 2, 3, \quad \psi = \frac{D_u k_c^\alpha - e_{11}}{\frac{e_{21}}{1 - k_d} - D_{vu}^T k_c^\alpha}.$$

In Eq. (15), via the orthogonality condition, the amplitude equation of model (4) under the first level of perturbation is obtained as follows:

$$\begin{aligned} (\varphi + \psi) \frac{\partial W_1}{\partial t_1} &= d_1 k_c^\alpha W_1 + 2(l_1 + \psi l_2) \overline{W}_2 \overline{W}_3, \\ (\varphi + \psi) \frac{\partial W_2}{\partial t_1} &= d_1 k_c^\alpha W_2 + 2(l_1 + \psi l_2) \overline{W}_1 \overline{W}_3, \\ (\varphi + \psi) \frac{\partial W_3}{\partial t_1} &= d_1 k_c^\alpha W_3 + 2(l_1 + \psi l_2) \overline{W}_1 \overline{W}_2, \end{aligned} \tag{18}$$

where $l_1 = p_{20}\varphi^2 + p_{11}\varphi$, $l_2 = q_{20}\varphi^2 + q_{11}\varphi + q_{02}$.

Solving Eq. (15), we get

$$\begin{aligned} \begin{pmatrix} u_2 \\ v_2 \end{pmatrix} &= \begin{pmatrix} U_0 \\ V_0 \end{pmatrix} + \sum_{j=1}^3 \begin{pmatrix} U_j \\ V_j \end{pmatrix} e^{i k_j \cdot r} + \sum_{j=1}^3 \begin{pmatrix} U_{jj} \\ V_{jj} \end{pmatrix} e^{i 2 k_j \cdot r} \\ &+ \begin{pmatrix} U_{12} \\ V_{12} \end{pmatrix} e^{i(k_1 - k_2) \cdot r} + \begin{pmatrix} U_{23} \\ V_{23} \end{pmatrix} e^{i(k_2 - k_3) \cdot r} + \begin{pmatrix} U_{31} \\ V_{31} \end{pmatrix} e^{i(k_3 - k_1) \cdot r} + \text{c.c.}, \end{aligned} \tag{19}$$

where

$$\begin{aligned} \begin{pmatrix} U_0 \\ V_0 \end{pmatrix} &= \begin{pmatrix} u_{00} \\ v_{00} \end{pmatrix} (|W_1|^2 + |W_2|^2 + |W_3|^2), \quad U_j = \varphi V_j, \\ \begin{pmatrix} U_{jj} \\ V_{jj} \end{pmatrix} &= \begin{pmatrix} u_{11} \\ v_{11} \end{pmatrix} W_j^2, \quad \begin{pmatrix} U_{ij} \\ V_{ij} \end{pmatrix} = \begin{pmatrix} u_* \\ v_* \end{pmatrix} W_i \overline{W}_j, \end{aligned}$$

with

$$\begin{aligned} \begin{pmatrix} u_{00} \\ v_{00} \end{pmatrix} &= \frac{-2}{\frac{e_{11}(e_{22}+k_p)}{1-k_d} - \frac{e_{12}e_{21}}{1-k_d}} \begin{pmatrix} \frac{l_1(e_{22}+k_p)}{1-k_d} - e_{12}l_2 \\ e_{11}l_2 - \frac{e_{21}l_1}{1-k_d} \end{pmatrix}, \\ \begin{pmatrix} u_{11} \\ u_{11} \end{pmatrix} &= - \begin{pmatrix} e_{11} - 4D_u k_c^\alpha & e_{12} - 4D_{uv} k_c^\alpha \\ \frac{e_{21}}{1-k_d} - 4D_{vu}^T k_c^\alpha & \frac{e_{22}+k_p}{1-k_d} - 4D_v k_c^\alpha \end{pmatrix}^{-1} \begin{pmatrix} l_1 \\ l_2 \end{pmatrix}, \\ \begin{pmatrix} u_* \\ u_* \end{pmatrix} &= -2 \begin{pmatrix} e_{11} - 3D_u k_c^\alpha & e_{12} - 3D_{uv} k_c^\alpha \\ \frac{e_{21}}{1-k_d} - 3D_{vu}^T k_c^\alpha & \frac{e_{22}+k_p}{1-k_d} - 3D_v k_c^\alpha \end{pmatrix}^{-1} \begin{pmatrix} l_1 \\ l_2 \end{pmatrix}. \end{aligned}$$

By applying the Fredholm solvability condition in Eq. (16), considering solutions (17) and (19) of the upper two levels of perturbation equations, we obtain the amplitude equation of model (4) under the second level of perturbation as follows:

$$\begin{aligned} (\varphi + \psi) \left(\frac{\partial Y_1}{\partial t_1} + \frac{\partial W_1}{\partial t_2} \right) &= k_c^\alpha (d_2 W_1 + d_1 Y_1) - [(I_1 + \psi S_1)|W_1|^2 \\ &\quad + (I_2 + \psi S_2)(|W_2|^2 + |W_3|^2)] W_1 \\ &\quad + 2(l_1 + \psi l_2)(\overline{W}_2 \overline{Y}_3 + \overline{W}_3 \overline{Y}_2), \\ (\varphi + \psi) \left(\frac{\partial Y_2}{\partial t_1} + \frac{\partial W_2}{\partial t_2} \right) &= k_c^\alpha (d_2 W_2 + d_1 Y_2) - [(I_1 + \psi S_1)|W_2|^2 \\ &\quad + (I_2 + \psi S_2)(|W_1|^2 + |W_3|^2)] W_2 \tag{20} \\ &\quad + 2(l_1 + \psi l_2)(\overline{W}_1 \overline{Y}_3 + \overline{W}_3 \overline{Y}_1), \\ (\varphi + \psi) \left(\frac{\partial Y_3}{\partial t_1} + \frac{\partial W_3}{\partial t_2} \right) &= k_c^\alpha (d_2 W_3 + d_1 Y_3) - [(I_1 + \psi S_1)|W_3|^2 \\ &\quad + (I_2 + \psi S_2)(|W_2|^2 + |W_1|^2)] W_3 \\ &\quad + 2(l_1 + \psi l_2)(\overline{W}_2 \overline{Y}_1 + \overline{W}_1 \overline{Y}_2), \end{aligned}$$

where

$$\begin{aligned} I_1 &= -(2\varphi p_{20} + p_{11})(u_{00} + u_{11}) - (\varphi p_{11} + 2p_{02})(v_{00} + v_{11}) \\ &\quad - 3p_{30}\varphi^3 - 3p_{21}\varphi^2 - 3p_{12}\varphi - 3p_{03}, \\ I_2 &= -(2\varphi p_{20} + p_{11})(u_{00} + u_*) - (\varphi p_{11} + 2b_{02})(v_{00} + v_*) \\ &\quad - 6p_{30}\varphi^3 - 6p_{21}\varphi^2 - 6p_{12}\varphi - 6b_{30}, \end{aligned}$$

$$\begin{aligned}
 S_1 &= -(2\varphi q_{20} + p_{11})(u_{00} + u_{11}) - (\varphi q_{11} + 2q_{02})(v_{00} + v_{11}) \\
 &\quad - 3q_{30}\varphi^3 - 3q_{21}\varphi^2 - 3q_{12}\varphi - 3q_{03}, \\
 S_2 &= -(2\varphi q_{20} + q_{11})(u_{00} + u_*) - (\varphi q_{11} + 2q_{02})(v_{00} + v_*) \\
 &\quad - 6q_{30}\varphi^3 - 6q_{21}\varphi^2 - 6q_{12}\varphi - 6q_{03}.
 \end{aligned}$$

The amplitude $A_j = A_j^u/\varepsilon = A_j^v$ is the coefficient of $e^{ik_j \cdot r}$ in each level:

$$\begin{pmatrix} A_j^u \\ A_j^v \end{pmatrix} = \varepsilon \begin{pmatrix} \varphi \\ 1 \end{pmatrix} W_j + \varepsilon^2 \begin{pmatrix} \varphi \\ 1 \end{pmatrix} Y_j + o(\varepsilon^2). \tag{21}$$

Then, we multiply Eqs. (18) and (20) by ε and ε^2 respectively, and use Eqs. (13) and (21) to combine the variables. Consequently the amplitude equation is gained as follows:

$$\begin{aligned}
 \tau_0 \frac{\partial A_1}{\partial t} &= \mu A_1 + g_0 \bar{A}_2 \bar{A}_3 - \varepsilon [g_1 |A_1|^2 + g_2 \varepsilon (|A_2|^2 + |A_3|^2 \varepsilon)] A_1, \\
 \tau_0 \frac{\partial A_2}{\partial t} &= \mu A_2 + g_0 \bar{A}_1 \bar{A}_3 - \varepsilon [g_1 |A_2|^2 + g_2 \varepsilon (|A_1|^2 + |A_3|^2 \varepsilon)] A_2, \\
 \tau_0 \frac{\partial A_3}{\partial t} &= \mu A_3 + g_0 \bar{A}_1 \bar{A}_2 - \varepsilon [g_1 |A_3|^2 + g_2 \varepsilon (|A_1|^2 + |A_2|^2 \varepsilon)] A_3,
 \end{aligned} \tag{22}$$

where

$$\begin{aligned}
 \tau_0 &= \frac{\varphi + \psi}{D_{vu}^T k_c^\alpha}, & \mu &= \frac{D_{vu} - D_{vu}^T}{D_{vu}^T}, \\
 g_0 &= \frac{l_1 + \psi l_2}{2D_{vu}^T k_c^\alpha}, & g_1 &= \frac{I_1 + \psi S_1}{D_{vu}^T k_c^\alpha}, & g_2 &= \frac{I_2 + \psi S_2}{D_{vu}^T k_c^\alpha}.
 \end{aligned}$$

5 Stability analysis of pattern formations

It is obviously that stable Turing patterns correspond to stable steady states, and each amplitude A_j can be decomposed into $A_j = \rho_j e^{i\theta_j}$ where θ_j is the phases angle, and magnitude $\rho_j = |A_j|$. Substituting $A_j = \rho_j e^{i\theta_j}$ into Eq. (22), one obtains the equations with respect to real variables ρ_j and θ_j as follows:

$$\begin{aligned}
 \tau_0 \frac{\partial \theta}{\partial t} &= -g_0 \frac{\rho_1^2 \rho_2^2 + \rho_2^2 \rho_3^2 + \rho_1^2 \rho_3^2}{\rho_1 \rho_2 \rho_3} \sin \theta, \\
 \tau_0 \frac{\partial \rho_1}{\partial t} &= \mu \rho_1 + |g_0| \rho_2 \rho_3 \cos \theta - g_1 \rho_1^3 - g_2 (\rho_2^2 + \rho_3^2) \rho_1, \\
 \tau_0 \frac{\partial \rho_2}{\partial t} &= \mu \rho_2 + |g_0| \rho_1 \rho_3 \cos \theta - g_1 \rho_2^3 - g_2 (\rho_1^2 + \rho_3^2) \rho_2, \\
 \tau_0 \frac{\partial \rho_3}{\partial t} &= \mu \rho_3 + |g_0| \rho_1 \rho_2 \cos \theta - g_1 \rho_3^3 - g_2 (\rho_1^2 + \rho_2^2) \rho_3,
 \end{aligned} \tag{23}$$

where $\theta = \theta_1 + \theta_2 + \theta_3$. Equation (23) has five types of solutions that correspond to specific pattern solutions. The following points are summarized:

(i) The homogeneous stationary state

$$(O: \rho_1 = \rho_2 = \rho_3 = 0)$$

is stable for $\mu < \mu_2 = 0$ and unstable for $\mu > \mu_2 = 0$.

(ii) The stripe pattern

$$\left(S: \rho_1 = \sqrt{\frac{\mu}{g_1}} \neq 0 \text{ and } \rho_2 = \rho_3 = 0 \right)$$

is stable for $\mu > \mu_3 = g_0^2 g_1 / (g_2 - g_1)^2$ and unstable for $\mu < \mu_3$.

(iii) The hexagon pattern

$$\left(I_0 \text{ or } I_\pi: \rho_1 = \rho_2 = \rho_3 = \frac{|g_0| \pm \sqrt{g_0^2 + 4(g_1 + 2g_2)\mu}}{2(g_1 + 2g_2)} \right)$$

exists for $\mu > \mu_1 = -g_0^2 / (4(g_1 + 2g_2))$. The solution

$$\rho^- = \frac{|g_0| - \sqrt{g_0^2 + 4(g_1 + 2g_2)\mu}}{2(g_1 + 2g_2)}$$

is always unstable, and the solution

$$\rho^+ = \frac{|g_0| + \sqrt{g_0^2 + 4(g_1 + 2g_2)\mu}}{2(g_1 + 2g_2)}$$

is stable only for $\mu < \mu_4 = g_0^2(2g_1 + g_2) / (g_2 - g_1)^2$.

(iv) The mixed state

$$\left(\rho_1 = \frac{|g_0|}{g_2 - g_1} \text{ and } \rho_2 = \rho_3 = \sqrt{\frac{\mu - g_1 \rho_1^2}{g_1 + g_2}} \right)$$

exists for $g_2 > g_1$ and $\mu > \mu_3 = g_0^2 g_1 / (g_2 - g_1)^2$ and is always unstable.

6 Numerical simulations

In this section, we carry on some numerical simulations to verify the theoretical results on pattern selections in Section 5 and the effect of D_{vu} and α on Turing instability and patterns in model (4). Also, by applying PD control tactics in model (4), we find that the PD control cannot only improve the instability driven by diffusion terms, but also change the pattern structure by choosing appropriate values of k_p and k_d . Because of the similar structure of Turing patterns between activating reactant u and inhibiting reactant v , we only give the pattern formation of u in this section.

The parameters of the controlled model (4) are selected as: $a = 0.04$, $q = 0.01$, $f = 0.5$, $D_u = D_v = 1$, $D_{uv} = 0$, and we choose D_{vu} as the bifurcation parameter. Through calculation, we have the equilibrium point $E^* = (u^*, v^*) = (0.5189, 0.5189)$ and $D_{vu}^T = 0.8098$. We can also obtain that the coefficients of the corresponding amplitude equation (22): $g_0 = -22.4671$, $g_1 = 1392.8$, $g_2 = 2957.1$, and the critical values of the appearance of various patterns: $\mu_1 = -0.0173$, $\mu_2 = 0$, $\mu_3 = 0.2873$, $\mu_4 = 1.1847$.

6.1 Pattern structure of model (4) without control

In this subsection, we only consider the effect of D_{vu} and α on the spatiotemporal dynamics in model (4). Let $k_p = k_d = 0$.

In order to sketch the Turing patterns for model (4), we adopt the time step size $\Delta t = 0.001$ and the space step size $d_x = d_y = 0.1$ over a two-dimensional domain uniformly divided into $[0, 600] \times [0, 600]$ lattice points. Select the bounded domain $\Omega = [0, L_x] \times [0, L_y]$ and apply homogeneous Neumann boundary conditions. The initial conditions of the experiments are chosen to be near the positive equilibrium point E^* , as follows:

$$u = u^* + 0.001 \cdot \sigma, \quad v = v^* + 0.001 \cdot \sigma,$$

where σ represents a uniformly distributed random perturbation.

We firstly consider the effect of D_{vu} on model (4) without control. In Fig. 4, we present the Turing patterns of model (4) with an iteration time of $t = 100$ and $\alpha = 2$, selecting $D_{vu} = 0.6, 0.877, 1.4,$ and $1.8,$ respectively. When $D_{vu} = 0.6,$ we can get $\mu = -0.2591 < \mu_2 = 0$ in this case, and the pattern structure is solid color structure, which means that model (4) is stable at equilibrium point E^* . As $D_{vu} = 0.877,$ we have $\mu = 0.0829 < \mu_3 = 0.2873,$ leading spot pattern structure. Let $D_{vu} = 1.4,$ and we obtain $\mu = 0.7287 < \mu_4 = 1.1847,$ causing spot and stripe pattern structure. When $D_{vu} = 1.8,$ we get $\mu = 1.2227 > \mu_4 = 1.1847,$ and the pattern structure turns into stripe pattern structure. These agree with our conclusions driven in Section 5.

For illustrating the effect of α on model (4), we also give the pattern structures of model (4) for $\alpha = 1.2$ and 1.5 with $t = 100$ in Fig. 5, respectively. The values of D_{vu} are the same as those given in Fig. 4. It is obviously that as the value of α decreases, the

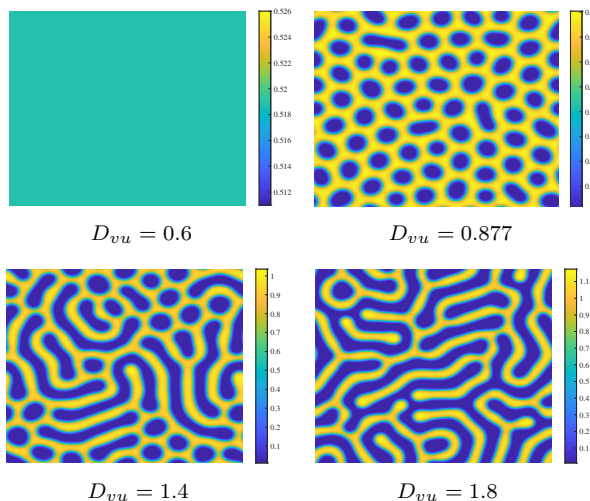


Figure 4. The pattern structure of model (4) without control for different values of the cross-diffusion coefficient D_{vu} .

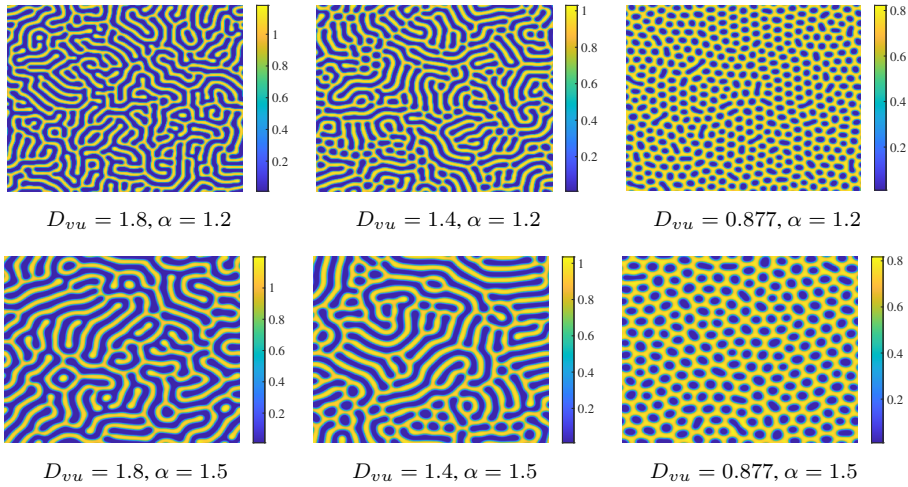


Figure 5. The pattern structure of model (4) without control for different values of the cross-diffusion coefficient D_{vu} and the fractional-diffusion coefficient α .

number of spots and strips increases significantly in the structure. The phenomenon is consistent with the previous conclusion, which verifies that when α is smaller, the range of Turing instability is wider. As shown in Fig. 5, under the same grid size, the smaller α , the more compact the pattern structure.

6.2 Pattern structure of model (4) under PD control

Then we discuss the PD controller’s influence on Turing patterns. Keeping all parameters given in Section 6, we conduct some numerical simulations on Turing patterns with different values of k_p and k_d .

Firstly, we apply controller’s parameter k_d to improve the Turing instability and change pattern structures of model (4). Let $k_p = 0$. Fix parameters $D_{vu} = 1.8$ and let $k_d = 0, 0.635, 0.775, \text{ and } 0.8$. According to expression (7) for D_{vu}^T , we obtain the corresponding $D_{vu}^T = 0.8098, 1.3539, 1.7717, \text{ and } 1.8959$, respectively.

Based on Theorem 2 and some driven conditions, when $D_{vu} > D_{vu}^T$, we have $h_{k_{\min}} < 0$, which is leading positive value of $\text{Re}(\lambda)$, so that the Turing instability of model (4) will occur. Otherwise, it will not occur. Then we plot the relationship between $\text{Re}(\lambda)$ and different values of k_d in Fig. 6. It is clearly that as the value of k_d increases, the value of $\text{Re}(\lambda)$ decreases gradually, and when $k_d = 0.8$, causing $D_{vu}^T = 1.8959 > D_{vu} = 1.8$, $\text{Re}(\lambda)$ keeps negative. It shows that the Turing instability of model (4) can be suppressed by k_d .

Then we give some simulations of the Turing pattern structures of model (4) with $\alpha = 2$. We can see from Fig. 7 that the PD controller has a significant regulation effect on the Turing pattern structure of oregonator model. When $k_d = 0$, which means that model (4) is uncontrolled, the pattern mode is stripe pattern structure. Then we choose

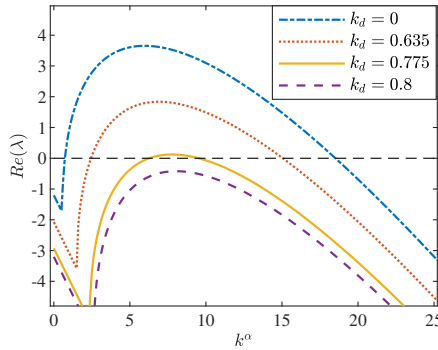


Figure 6. The graphic of $Re(\lambda)$ against k^α for different parameters $k_d = 0, 0.635, 0.775,$ and 0.8 .

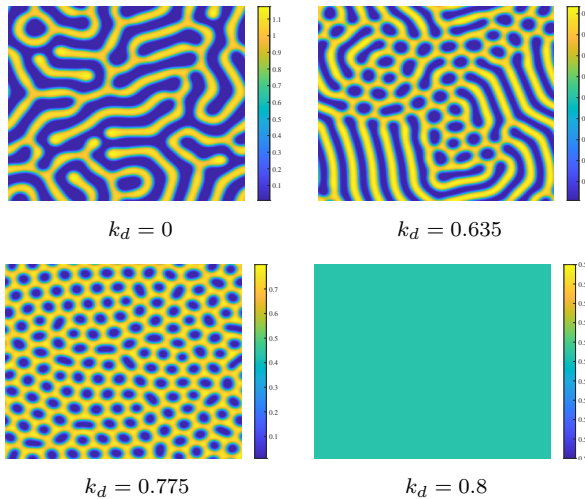


Figure 7. The pattern structures of model (4) under PD control with $k_d = 0.635, 0.775,$ and 0.8 .

$k_d = 0.635$, and it turns into spot and stripe pattern structure. As we increase the value of k_d to 0.775 and 0.8 , the pattern continues to change into spot pattern structure and solid pattern structure, respectively. It is clearly that we can realize the transformation of pattern structure and achieve stability of model (4) caused by cross-diffusion term via changing the value of k_d .

Following that, we consider the PD controller’s parameter k_p . Let $k_d = 0$ and keep other parameters. Under the effect of PD controller for $k_p = -5.4$ and -6 , we can also achieve the transformation of pattern structures in model (4) with $\alpha = 2$ as shown in Fig. 8. Contrasting with Fig. 4, we can see that the stripe pattern structure turns into spot and stripe pattern structure ($k_p = -5.4$) and spot pattern structure ($k_p = -6$). Figure 8 indicates that k_p can also influence the pattern structure in model (4) like k_d . Also, the relationship between $Re(\lambda)$ and different values of k_p is plotted in Fig. 9.

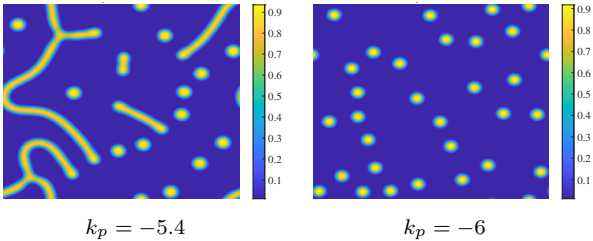


Figure 8. The pattern structures of model (4) under PD control with $k_p = -5.4$ and -6 .

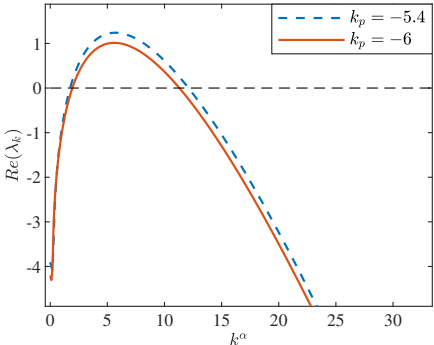


Figure 9. The graphic of $Re(\lambda)$ against k^α for different parameters $k_p = -5.4$ and -6 .

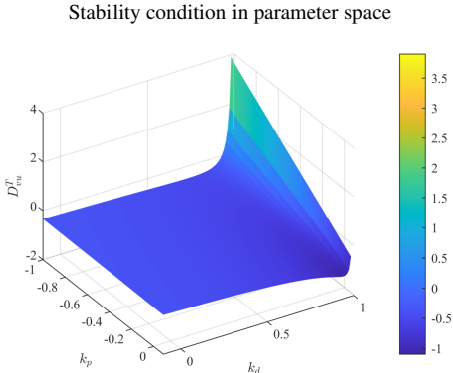


Figure 10. Graph of Turing bifurcation threshold D_{vu}^T varying with control parameters k_p and k_d .

Finally, we plot the relationship between controller parameters k_p, k_d and Turing bifurcation D_{vu}^T in Fig. 10 for comparing their control effects. From the result in Fig. 10 it is obviously that k_d has a more significant impact on improving bifurcation threshold than k_p . It corresponds with some numerical simulations presented above.

7 Conclusions

In this paper, we firstly introduce fractional-order diffusion terms into a bivariate oregonator model, then we apply a PD controller in this model. Choosing D_{vu} as the Turing bifurcation parameter, we discuss the condition when Turing instability occurs in the model, and give the bifurcation threshold. Also, we push the amplitude equation of the model, and the formation of pattern structure is predicted theoretically. Based on the theoretical analysis and numerical simulations, we verify the influence of fractional-order parameter α on the range of Turing instability caused by cross-diffusion term and the significant effect of PD controller on Turing instability and pattern structures. Selecting smaller value of α will make the model generate Turing instability earlier and the intensive pattern structure with the same D_{vu} . By choosing appropriate value of k_p or k_d , we achieve the suppression of Turing instability and transformation of pattern structures in oregonator model.

In the future, we will continue to explore the pattern selection mode of oregonator model and the derivation of amplitude equation in three-dimensional space, aiming to contribute more achievements to the study of nonlinear space–time dynamics.

Acknowledgment. The authors wish to express their gratitude to the editors and the reviewers for the helpful comments.

References

1. Z. Abbasi, I. Zamani, A.H.A. Mehra, M. Shafieirad, A. Ibeas, Optimal control design of impulsive SQUEIR epidemic models with application to COVID-19, *Chaos Solitons Fractals*, **139**:110054, 2020, <https://doi.org/10.1016/j.chaos.2020.110054>.
2. R.S.S. Baghel, J. Dhar, Pattern formation in three species food web model in spatiotemporal domain with Beddington–DeAngelis functional response, *Nonlinear Anal. Model. Control*, **19**(2):155–171, 2014, <https://doi.org/10.15388/NA.2014.2.1>.
3. I. Berenstein, C. Beta, Spatiotemporal chaos arising from standing waves in a reaction-diffusion system with cross-diffusion, *J. Chem. Phys.*, **136**(3), 2012, <https://doi.org/10.1063/1.3676577>.
4. I. Berenstein, C. Beta, Cross-diffusion in the two-variable Oregonator model, *Chaos*, **23**(3), 2013, <https://doi.org/10.1063/1.4816937>.
5. M. Bhuvaneswari, S. Eswaramoorthi, S. Sivasankaran, Cross-diffusion effects on MHD mixed convection over a stretching surface in a porous medium with chemical reaction and convective condition, *Eng. Trans.*, **67**(1):3–19, 2019, <https://doi.org/10.24423/EngTrans.820.20190308>.
6. D.W. Ding, X.Y. Zhang, J.D. Cao, N. Wang, D. Liang, Bifurcation control of complex networks model via PD controller, *Neurocomputing*, **175**:1–9, 2016, <https://doi.org/10.1016/j.neucom.2015.09.094>.
7. V. Duffet, J. Boissonade, Conventional and unconventional Turing patterns, *J. Chem. Phys.*, **96**(1):664–673, 1992, <https://doi.org/10.1063/1.462450>.

8. E. Dulos, J. Boissonade, J.J. Perraud, B. Rudovics, P.D. Kepper, Chemical morphogenesis: Turing patterns in an experimental chemical system, *Acta Biotheor.*, **44**(3–4):249–261, 1996, <https://doi.org/10.1007/BF00046531>.
9. F. Feng, J. Yan, F.-C. Liu, Y.-F. He, Pattern formation in superdiffusion Oregonator model, *Chin. Phys. B*, **25**(10):197–201, 2016, <https://doi.org/10.1088/1674-1056/25/10/104702>.
10. R.J. Field, R.M. Noyes, Oscillations in chemical systems. IV. Limit cycle behavior in a model of a real chemical reaction, *J. Chem. Phys.*, **60**(5):1877–1884, 1974, <https://doi.org/10.1063/1.1681288>.
11. A. Giri, S.P. Jain, S. Kar, Alteration in cross diffusivities governs the nature and dynamics of spatiotemporal pattern formation, *ChemPhysChem*, **21**(14):1608–1616, 2020, <https://doi.org/10.1002/cphc.202000142>.
12. J. Gjorgjieva, J. Jacobsen, Turing patterns on growing spheres: The exponential case, *Discrete Contin. Dyn. Syst.*, **2007**(Suppl.):436–445, 2007, <https://doi.org/10.3934/proc.2007.2007.436>.
13. D. Hernández, C. Varea, R.A. Barrio, Dynamics of reaction-diffusion systems in a subdiffusive regime, *Phys. Rev. E*, **79**(2):026109, 2009, <https://doi.org/10.1103/PhysRevE.79.026109>.
14. J. Horváth, I. Szalai, P.D. Kepper, An experimental design method leading to chemical Turing patterns, *Science*, **324**(5928):772–775, 2009, <https://doi.org/10.1126/science.1169973>.
15. C. Huang, X. Song, B. Fang, M. Xiao, J. Cao, Modeling, analysis and bifurcation control of a delayed fractional-order predator–prey model, *Int. J. Bifurcation Chaos*, **28**(09):1850117, 2018, <https://doi.org/10.1142/S0218127418501171>.
16. T.A.M. Langlands, B.I. Henry, S.L. Wearne, Turing pattern formation with fractional diffusion and fractional reactions, *J. Phys. Condens. Matter*, **19**(6):065115, 2007, <https://doi.org/10.1088/0953-8984/19/6/065115>.
17. S.B. Li, J.H. Wu, Y.Y. Dong, Turing patterns in a reaction-diffusion model with the Degr–Harrison reaction scheme, *J. Differ. Equations*, **259**(5):1990–2029, 2015, <https://doi.org/10.1016/j.jde.2015.03.017>.
18. Y. Nec, A.A. Nepomnyashchy, A.A. Golovin, Oscillatory instability in super-diffusive reaction–diffusion systems: Fractional amplitude and phase diffusion equations, *Europhys. Lett.*, **82**(5):58003, 2008, <https://doi.org/10.1209/0295-5075/82/58003>.
19. R. Peng, F.Q. Sun, Turing pattern of the Oregonator model, *Nonlinear Anal., Theory Methods Appl.*, **72**(5):2337–2345, 2010, <https://doi.org/10.1016/j.na.2009.10.034>.
20. R. Ruiz-Baier, C.R. Tian, Mathematical analysis and numerical simulation of pattern formation under cross-diffusion, *Nonlinear Anal., Real World Appl.*, **14**(1):601–612, 2013, <https://doi.org/10.1016/j.nonrwa.2012.07.020>.
21. C.R. Tian, Z.G. Lin, M. Pedersen, Instability induced by cross-diffusion in reaction–diffusion systems, *Nonlinear Anal., Real World Appl.*, **11**(2):1036–1045, 2010, <https://doi.org/10.1016/j.nonrwa.2009.01.043>.
22. A.M. Turing, The chemical basis of morphogenesis, *Bull. Math. Biol.*, **52**:153–197, 1990, <https://doi.org/10.1007/BF02459572>.

23. J.J. Tyson, P.C. Fife, Target patterns in a realistic model of the Belousov–Zhabotinskii reaction, *J. Chem. Phys.*, **73**(5):2224–2237, 1980, <https://doi.org/10.1063/1.440418>.
24. V.K. Vanag, I.R. Epstein, Cross-diffusion and pattern formation in reaction–diffusion systems, *Phys. Chem. Chem. Phys.*, **11**(6):897–912, 2009, <https://doi.org/10.1039/B813825G>.
25. C. Varea, J.L. Aragon, R.A. Barrio, Turing patterns on a sphere, *Phys. Rev. E*, **60**(4):4588, 1999, <https://doi.org/10.1103/PhysRevE.60.4588>.
26. R.D. Vigil, Q. Ouyang, H.L. Swinney, Turing patterns in a simple gel reactor, *Physica A*, **188**(1–3):17–25, 1992, [https://doi.org/10.1016/0378-4371\(92\)90248-0](https://doi.org/10.1016/0378-4371(92)90248-0).
27. J.P. Voroney, A.T. Lawniczak, R. Kapral, Turing pattern formation in heterogenous media, *Physica D*, **99**(2–3):303–317, 1996, [https://doi.org/10.1016/S0167-2789\(96\)00132-7](https://doi.org/10.1016/S0167-2789(96)00132-7).
28. C. Xu, W. Ou, Q. Cui, Y. Pang, M. Liao, J. Shen, M.Z. Baber, C. Maharajan, U. Ghosh, Theoretical exploration and controller design of bifurcation in a plankton population dynamical system accompanying delay, *Discrete Contin. Dyn. Syst., Ser. S*, 2024, <https://doi.org/10.3934/dcdss.2024036>.
29. X.-P. Yan, P. Zhang, C.-H. Zhang, Turing instability and spatially homogeneous Hopf bifurcation in a diffusive Brusselator system, *Nonlinear Anal. Model. Control*, **25**(4):638–657, 2020, <https://doi.org/10.15388/namc.2020.25.17437>.
30. Y. Yang, Y. Du, Spatiotemporal dynamics of a diffusive nutrient-phytoplankton model with delayed nutrient recycling, *Nonlinear Anal. Model. Control*, **29**(2):305–329, 2024, <https://doi.org/10.15388/namc.2024.29.34380>.
31. S. Zhao, H. Wang, W. Jiang, Turing–Hopf bifurcation and spatiotemporal patterns in a Gierer–Meinhardt system with gene expression delay, *Nonlinear Anal. Model. Control*, **26**(3):461–481, 2021, <https://doi.org/10.15388/namc.2021.26.23054>.
32. Y. Zhao, C. Xu, Y. Xu, J. Lin, Y. Pang, Z. Liu, J. Shen, Mathematical exploration on control of bifurcation for a 3D predator-prey model with delay, *AIMS Math.*, **9**(11):29883–29915, 2024, <https://doi.org/10.3934/math.20241445>.
33. P. Zhu, M. Xiao, X. Huang, F. Zhang, Z. Wang, J. Cao, Spatiotemporal dynamics optimization of a delayed reaction–diffusion mussel–algae model based on PD control strategy, *Chaos Solitons Fractals*, **173**:113751, 2023, <https://doi.org/10.1016/j.chaos.2023.113751>.
34. Q. Zhu, X. Yang, L.-X. Yang, C. Zhang, Optimal control of computer virus under a delayed model, *Appl. Math. Comput.*, **218**(23):11613–11619, 2012, <https://doi.org/10.1016/j.amc.2012.04.092>.